We are IntechOpen, the world's leading publisher of Open Access books Built by scientists, for scientists

5,300
Open access books available

130,000
International authors and editors

155M
Downloads

Our authors are among the

154
Countries delivered to

TOP 1%
most cited scientists

12.2%
Contributors from top 500 universities

CLARIVATE ANALYTICS BOOK CITATION INDEX INDEXED

WEB OF SCIENCE™

Selection of our books indexed in the Book Citation Index in Web of Science™ Core Collection (BKCI)

Interested in publishing with us?
Contact book.department@intechopen.com

Numbers displayed above are based on latest data collected.
For more information visit www.intechopen.com

Chapter

Beyond Mapping Functions and Gradients

Jean-Pierre Barriot and Peng Feng

Abstract

Mapping functions and gradients in GNSS and VLBI applications were introduced in the sixties and seventies to model the microwave propagation delays in the troposphere, and they were proven to be the perfect tools for these applications. In this work, we revisit the physical and mathematical basis of these tools in the context of meteorology and climate applications and propose an alternative approach for the wet delay part. This alternative approach is based on perturbation theory, where the base case is an exponential decay of the wet refractivity with altitude. The perturbation is modeled as a set of orthogonal functions in space and time, with the ability to separate eddy-scale variations of the wet refractivity.

Keywords: GNSS meteorology, positioning, VLBI, deep space tracking, neutral delays, mapping functions, gradients

1. Introduction

The effect of the Earth atmosphere on the propagation of light was noticed just after the invention of the telescope by Galileo Galilei, and tables of atmospheric refraction (bending of ray lights) were already available in the XVII century. After the advent of VLBI observations in the fifties and the launch of the first Earth satellite in the sixties, the modeling of the time delays caused by the neutral atmosphere became a necessity.

The current mathematical structure of the modeling of the propagation time delays, used in almost all GNSS software is given by [1].

$$\begin{aligned}\delta L(e_0) = m_h(e_0)\left[L_z^h + cotg(e_0)(G_N^h \cos(\varnothing) + G_E^h \sin(\varnothing)\right] \\ + m_w(e_0)\left[L_z^w + cotg(e_0)\left(G_N^w \cos(\varnothing) + G_E^w \sin(\varnothing)\right]\right.\end{aligned} \tag{1}$$

where δL is the slant (extra) delay with respect to propagation in vacuum along the bended ray, L_z^h and, L_z^w are the hydrostatic and wet zenith delays, e_0 and $\varnothing$ are the satellite elevation and azimuth angles as seen from the station, respectively; G_N^h and G_N^w, G_E^h and G_E^w are the north and east components of the hydrostatic and wet delays gradients; m_h and m_w are the hydrostatic and wet mapping functions. Eq. (1) is used in precise GNSS processing software through the modeling of the phase signal [2–4].

The mapping functions "map" the so-called slant neutral atmosphere (extra) delay δL (i.e. the delay along the bended ray from the observer to the emitter) to two "zenithal delays", named hydrostatic delay (very often improperly called "dry"

delay) L_z^h and wet delay L_z^w, essentially caused by the water vapor. The mapping functions are usually written [5] in the form of continuous fractions, that were introduced by Marini [6, 7] and normalized by Herring [8] in the form

$$m(e_0) = \frac{1 + \frac{a}{1+\frac{b}{1+c}}}{\sin(e_0) + \frac{a}{\sin(e_0)+\frac{b}{\sin(e_0)+c}}} \tag{2}$$

Other (simplified) forms of the mapping functions can be found in the literature [9], but the mainstream form is always Eq. (2). The gradients themselves, noted by the upper case letter G in Eq. (1) were introduced to compensate azimuthal anisotropic effects [10–12].

For the last thirty years, the improvements on these formulas mainly focused on better and better determinations of the coefficients a, b, c, by comparisons of these formulas with ray tracing. The literature acknowledges as "best" models the VMF1 and VMF3 families, with some seasonally adjusted coefficients constrained from ray-tracing results with respect to Numerical Weather Models (NWM) [13, 14].

The role of the water vapor in the neutral delay is important, as it can be up to 20% (about 45 cm of the zenithal delay L_z^w), with respect to the total zenithal delay $L_z^h + L_z^w$ (about 2.3 m). The other gases, including carbon dioxide, have a negligible role in the neutral delay [9, 15], thus cannot be detected through GNSS processing.

Water is present in its three phases on Earth atmosphere, hydrosphere and continents: solid, liquid and water vapor, with important latent heats between phases. Water vapor in the atmosphere has large sources (evaporation, evapotranspiration) and sinks (rain, snow). Water vapor is also the most important greenhouse gas (beyond carbon dioxide) and the driver of cloud coverage. To describe the water cycle [16] is therefore of the uttermost importance, as evidenced by the so-called Energy Balance models [17, 18] that can be written

$$C_1 S_0 (1 - \alpha) = C_2 \frac{dT}{dt} + C_3 T^4 (1 - \beta) \tag{3}$$

Where S_0 is the solar constant (1360 W/m^2), T is the mean temperature on the Earth surface in Kelvin, t is the time. C_1, C_2 and C_3 are constants.

The coefficients α and β are albedos, respectively in the visible and infrared wavelengths, both mainly driven by the water vapor contents of the Earth atmosphere [19]. The coefficients α reflects the cloud coverage, typically today at the 30% level, and the coefficient β is an infrared albedo, keeping our planet warm at around 15 °C. Without the greenhouse gases, our planet will be at a freezing mean temperature of −18 °C. They have antagonist effects, an increase of α means a cooling of Earth surface, and an increase of β means a warming, with a lot of intricacies between the positive and negative feedbacks related to the water vapor cycle of the climate models [20]. The ultimate goal of global long-term climate models [21] is to predict which effect will prevail (this is the dT/dt term in the right side of Eq. (3)).

The study [22] highlights the difficulty of measuring atmospheric water vapor with sufficient spatial and temporal resolution, and with sufficient accuracy, to provide observational constraints. GNSS processing is not the only source of water vapor data in the atmosphere. Remote sensing by satellites is the main provider [23], but the resolution of their data sets is limited by the distance between the satellites and the Earth and their orbital cycles. Besides, satellites are expensive. GNSS receivers, even precise ones, are a lot cheaper, and can provide long-term time series with high temporal resolution. Other ground-based instruments are

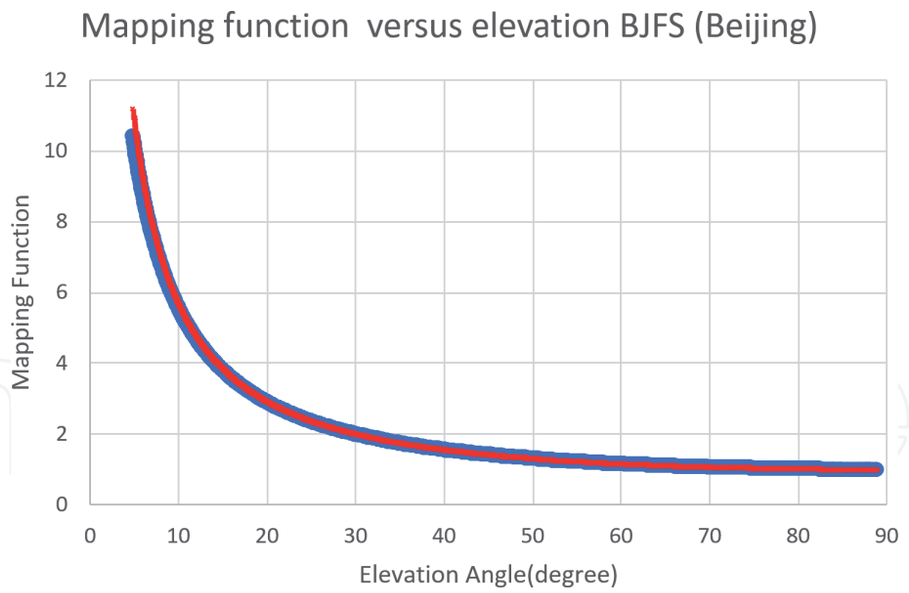

Figure 1.
The mapping functions m_h (blue) and m_w (red) plotted against each other for a typical GNSS station in Beijing (latitude: 39.6086° N, longitude: 115.8922° E), winter time on January 16th, 2012, with the VMF1 model [13], parameterized by inputting data from the ECMWF numerical weather model EAR-40 [31].

mainly lidars [24], photometers [25], and water vapor radiometers [26]. The only source providing *in situ* meteorological data are the radiosondes [27], launched twice per day in a limited amount of worldwide sites. Many studies have been devoted to the causal relationship between water vapor and rain [28, 29], including extreme events [30].

It is therefore important to separate the water vapor modeling coefficients L_z^w, G_N^w and G_E^h from the hydrostatic coefficients L_z^h, G_N^h and G_E^h in Eq. (1). But this is easier said than done, as the functions $m_h(e_0)$ and $m_w(e_0)$ in Eq. (1) have almost the same dependence on the elevation angle e_0 (see **Figure 1**).

2. Basic assumptions at the core of the definition of mapping functions and gradients

Mapping functions, as they were introduced by Marini [6, 32] are based on the assumption of a totally layered atmosphere. This means that the refractivity n is only a function of height (the exact meaning of the word height is related to the definition of geoid). The ray equation of radio waves (including light) obeys, in the spherical approximation and again for a totally layered atmosphere (dependence on geocentric radius r of the refractivity n), the prime integral relation

$$n(r)\, r \cos(\mathrm{e}) = n(r_0) r_0 \cos(e_0) \tag{4}$$

where r is the geocentric radius, r_0 is the geocentric radius at the receiver location, $n(r)$ is the refractivity at geocentric radius r, e is the angle between the tangent to the bended ray and the local horizon (the plane perpendicular to the direction of r at height r). e_0 is the elevation angle of the tangent of the bended ray at the receiver location.

The details of the computation of the ray path can be found in [6, 33, 34]. The refractivity of the atmosphere is a function of pressure, temperature and water vapor contents. A formula widely used is the Smith and Weintraub formula [35], derived for laboratory conditions (air perfectly mixed), as

$$(n-1) = K_1 \frac{P_d}{T} + K_2 \frac{e}{T} + K_3 \frac{e}{T^2} \tag{5}$$

where P_d is the partial pressure of dry air in millibars, T is the temperature in Kelvin, e is the partial pressure of water vapor. K_1, K_2 and K_3 are constants. The P_d term corresponds to the "dry" part of the refractivity, the e terms correspond to the "wet" part of the refractivity. Many authors have improved the coefficients K_1, K_2 and K_3 year after year [15, 36, 37].

This formula can be easily rewritten as

$$(n-1) = K_1' \frac{P}{T} + K_2' \frac{e}{T} + K_3 \frac{e}{T^2} \tag{6}$$

Where $P = P_d + e$. This rewriting, was the first term is denominated as the hydrostatic component of the refractivity, was proposed by Davis et al. [7] and then has been widely accepted, but lead to a track of confusion in the literature between the meaning of "hydrostatic" and "dry". The word "hydrostatic" has specifically no meaning in Eq. (6), other than indicating that the total pressure is used instead of the partial pressure of the non-wet (dry) air, as in Eq. (5). The word "hydrostatic" has a precise meaning in numerical weather models [38], where it indicates that the equilibrium of an air column is a balance between the vertical pressure gradient and the buoyancy forces, neglecting convective processes [39] as a simplification of the Navier–Stokes primitive Equations [40]. This is also the assumption made in the Saastamoinen model of the atmosphere propagation delays [41], with the total pressure P at ground level taken as a parameter (and with also the assumption of an atmosphere "at rest").

To a good degree of approximation, the refractivity of air obeys a twofold exponential formula [42].

$$n(r) = 1. + \delta n_h + \delta n_w = 1. + N_h \exp\left(\frac{r - r_0}{H_h}\right) + N_w \exp\left(\frac{r - r_0}{H_w}\right) \tag{7}$$

The terms N_h, H_h and N_w, H_w have, respectively, a value of $250 \cdot 10^{-6}$, 8.7 km, $128 \cdot 10^{-6}$ and 2.7 km for the location of our geodesy observatory in Tahiti (from the fit of radiosounding data over a typical year). The scale height H_w varies from 1.5 km to up to 8 km from place to place and according to a seasonal cycle [43]. For all practical GNSS purposes, one can consider that the water vapor is concentrated in the troposphere (from 8 km over the poles to 18 km at the Equator [44, 45], and that the atmosphere extends up to 100 km [46, 47]. The International Union of Telecommunications [48] recommends the use, for radio-link purposes, on a worldwide basis and for altitudes taken from sea level, of the formula (7), with N_h = $315 \cdot 10^{-6}$, H_h = 7.35 km, the wet part being omitted (it is in fact included as a worldwide average in N_h and H_h).

The prime integral (4) allows two things: 1/the computation of the path, 2/the computation of the time delay along the path as

$$L = \int_{path} n \, ds \tag{8}$$

The extra delay (in equivalent length) caused by the atmosphere is

$$\delta L = \int_{path} (n-1) \, ds \tag{9}$$

By inserting Eq. (6) into Eq. (9) we get the separation of δL into additive "hydrostatic" δL_h and "wet" δL_w delays. The ratios of δL_h and δL_w with respect to the corresponding values taken along a vertical path are by definition (as in Eq. (1)) the hydrostatic (m_h) and wet (m_w) mapping functions that only depend on the elevation angle e_0 of the tangent of the bended ray at the receiver location.

Davis et al. [10] pushed the physical analysis of Eq. (9) a little bit further by introducing the notion of gradients. This notion is also based on the basic assumption of a main dependence of the refractivity with respect to height, with the refractivity in the neighborhood of the receiver written as

$$n = n_V(r) + small\ lateral\ terms \tag{10}$$

where r is taken along the local vertical of the receiver, and n_V is the variation of n along the vertical of the observation site (the value of n at the receiver station is $n(r_0) = n_V(r_0)$). One can note that this writing violates, on a pure mathematical ground the dependence of n on only the geocentric radius, that was assumed for the computation of the path in Eq. (4) (i.e. no small lateral terms should be present). If we define a local frame with units vector $(\hat{x}, \hat{y})$ in the tangent plane perpendicular to the vertical direction of the station (usually defined by the North and East directions as in Eq. (1), we get, with also the assumption of a "flat Earth", the approximation

$$n\ (r; x, y) \simeq n_V(r) + \left(\frac{\partial n}{\partial x}\right)_{(r)} x + \left(\frac{\partial n}{\partial y}\right)_{(r)} y \tag{11}$$

This is nothing else than a Taylor series, meaning that x and y are assumed to be small, and the subscript (r) emphasizes that the partial derivatives of n are varying with the height r (i.e. they are not taken at $r = r_0$). For low elevation angles of the path, x and y are by no means "small", and can reach up to several hundreds of kilometers. We can define Eq. (11) as a "cylindrical" expansion of the refractivity.

If we insert this in Eq. (9), we get

$$\delta L(e_0) = \int_{path} (n_V - 1)\, ds + \int_{path} \left(\frac{\partial n}{\partial x}\right)_{(r)} x\, ds + \int_{path} \left(\frac{\partial n}{\partial y}\right)_{(r)} y\, ds \tag{12}$$

If we now divide the first right term of Eq. (12) by

$$\delta L(e_0) = \int_{vertical} (n_V - 1)\, ds \tag{13}$$

We get

$$\delta L(e_0) = m(e_0) \int_{vertical} (n_V - 1)\, ds + \int_{path} \left(\frac{\partial n}{\partial x}\right)_{(r)} x\, ds + \int_{path} \left(\frac{\partial n}{\partial y}\right)_{(r)} y\, ds \tag{14}$$

where $m(e_0) \approx \frac{1}{\sin e_0}$ is by definition the mapping function. The value $\frac{1}{\sin e_0}$ is obtained by setting all the coefficients $a, b, c \ldots$ to 0 in Eq. (2).

By writing $R^2 = x^2 + y^2$, $x = R\cos\phi$, $y = R\sin\phi$, and taking advantage of the fact that the path is nearly a straight line, as n is close to 1 at a 10^{-3} level, we can write, for the two integrals involving the derivatives of n, $R = rcotg(e_0)$ and $ds = \frac{dr}{\sin(e_0)}$. This is permissible, because physically these derivatives, as well as x and y are assumed to be small quantities. We obtain for the integral relative to the partial derivative $\left(\frac{\partial n}{\partial x}\right)$

$$\int_{path} \left(\frac{\partial n}{\partial x}\right)_{(r)} x\, ds = m(e_0) \cot e_0 \cos\phi \int_{r=r_0}^{r_{top}} \left(\frac{\partial n}{\partial x}\right)_{(r)} r\, dr \tag{15}$$

where r_{top} is the top of the atmosphere with respect to the geocentric radius (around 100 km), and a similar expression in $\sin\phi$ for the partial derivative $\left(\frac{\partial n}{\partial y}\right)$.

The precise details of the mathematical machinery linking Eq. (11) to Eq. (1) can be found in Davis et al. [10]. The important fact, from a physical point-of-view is that, if we split the refractivity into a "hydrostatic" and a "wet" part, we get the "hydrostatic" and "wet" gradients of Eq. (1) as

$$G_N^h = \int_{r=r_0}^{r_{top}} \left(\frac{\partial n_h}{\partial x}\right)_{(r)} r\, \mathrm{dr}, G_E^h = \int_{r=r_0}^{r_{top}} \left(\frac{\partial n_h}{\partial y}\right)_{(r)} r\, \mathrm{dr} \tag{16}$$

$$G_N^w = \int_{r=r_0}^{r_{top}} \left(\frac{\partial n_w}{\partial x}\right)_{(r)} r\, \mathrm{dr}, G_E^w = \int_{r=r_0}^{r_{top}} \left(\frac{\partial n_w}{\partial y}\right)_{(r)} r\, \mathrm{dr} \tag{17}$$

The significations of the gradients are therefore the integration, along the altitude, weighted by the altitude, of the North and East directional derivatives of the "hydrostatic" and "wet" parts of the refractivity, evaluated along the vertical of the receiver location. It is in fact an integration along the geometrical line-of-sight.

3. Physical meaning of zenithal delays and gradients

The modeling of the extra-delays caused by the atmosphere by the combination of mapping functions and gradients of Eq. (1) has proved very effective since Davis introduced his formula 30 years ago [49–51]. But what is the real meaning of effective?

We have to remember that this model was primarily introduced to model atmospheric delays in VLBI, then to improve positioning estimates from GNSS data, and it is now battle-proven for these two applications. But another application, being known today as GNSS meteorology, emerged during the nineties, first with the modeling of the integrated water vapor contents along the vertical of the GNSS receiver (i.e. no gradients), known as "precipitable water" (or PW), that used the L_z^w zenithal delay converted to PW through a multiplicative constant, known as the Π constant introduced by Bevis et al. [52]. Because the wet and dry mapping functions cannot be separated, for any practical purposes, in Eq. (1), the separation between the sum $L_z^d + L_z^w$ and L_z^w must be done by introducing an "external hydrostatic estimate" L_z^h, the model of choice being the so-called Saastamoinen model [41]. By its own inception, a PW time series is relative to a particular GNSS station, and does not provide any information about the lateral gradients of the water vapor contents of the atmosphere for this site. But a dense network of GNSS receivers do. An even more powerful way to grasp the 3D and even 4D (with the inclusion of time) variations of the water vapor contents of the atmosphere is the tomography, first promoted by [1, 53, 54]. In the approach of tomography, Eq. (1) is just seen as an intermediate tool, the data inputted in the tomography software being the reconstructed δL^w (the "wet" part of Eq. (1)). The tomography approach needs a dense network of GNSS receivers over a limited area, and take advantage of a multiple crossing paths between the receivers and the satellites of the GNSS constellations to invert the intrinsically ill-posed correspondence between the δL^w and the 3D atmospheric water vapor refractivity field over the area.

All the tomography software treat, to obtain a tractable problem, the rays as straight lines. This means that low-elevation slant delays cannot be considered.

Some authors [51, 55, 56] tried to assess the physical meaning of tropospheric gradients, but their effort were limited to qualitative assessments and correlations studies. Up to our knowledge [57], nobody is using gradients as data to constraint operational NWMs, albeit efforts having made to extract gradients from NWM numerical simulations [14] or make comparisons with NWMs outputs [58], or even to propose the use of slant delays for such a use [59]. The only GNSS data products that are currently inputted (assimilated) in NWMs are total zenithal delays (i.e. the sum $L_z^d + L_z^w$), as for example in the latest Météo-France AROME model [60].

This is clearly sending the message that the meteorology community does not yet consider gradients as a usable data set. We think that the main reason for this is the underlying assumption of the cylindrical Taylor's expansion [Eq. (11)], at the basis of the notion of gradients, where a strict separation between vertical variations and lateral variations is assumed, and supposed valid over all the troposphere (at least as seen from the receiver location). This assumption is closely related to the hydrostatic assumption, itself closely linked to the highly non-linear Navier–Stokes equations, which admit as solutions a combination of laminar and turbulent/convective flows. At scales larger than a few tens of kilometers, the atmospheric flows are mostly horizontal [61]. This corresponds to the highest resolution available for typical MNW models, built around the hydrostatic assumption [62]. The atmospheric turbulence [63] itself is organized as "vortices", or eddies, with scales varying over several orders of magnitude, from a few meters to several hundreds of kilometers [64, 65]. A combination of laminar and turbulence is also possible, and it is known as "frozen flow", where "frozen turbulence" is carried by laminar flow [66]. This is illustrated for the layman by clouds driven by the wind. Atmospheric turbulence/convection is modeled through statistical tools, the structure functions [67], that obeys an exponential decay with altitude (i.e. turbulence is "higher" in the boundary layer) [68]. The definition of gradients by Davis et al. [10] is simply too crude from a "meteorological" point-of-view.

4. Beyond zenithal delays and gradients

Therefore, what can be the future of the modeling of neutral delays in GNSS meteorology? Applications in GNSS positioning and VLBI clearly show that Eq. (1) is sufficient for these applications, because what is of interest to these users are the integrated delays, not directly the variations of refractivity in the atmosphere. Eq. (1) is sufficient by itself to model these slant (extra) delays, as evidenced by tomography applications and the statistical analysis of these delays [69]. The zenithal total delays have proven to have a physical meaning, as they are related to the modeling of PW through an a priori model of the "dry" atmosphere and a proportional correspondence to zenithal wet delays. They are also feeding the current medium resolution NWM models. The gradients themselves are more questionable. They are merely *ad'hoc*, empirical corrections introduced for positioning and VLBI applications.

Can the definition of gradients be improved? From a physical point-of-view, we do not think so. The main assumption to derive the delay gradients in Davis et al. formula (Eqs. (16) and (17)) is an integration, along the line-of-sight receiver-satellite, of the gradients of the refractivity. Even with a better "geometrical definition" of the gradients, taking into account the curvature of Earth, the bending of the rays, etc. ... , the main problem is that a line-of-sight station-satellite usually cross – and average– many eddies. According to [70], the shape and size of the eddies

depend on the altitude. Close to the ground (0–2 km of altitude), the eddies are assumed to be small and not far from isotropic, while the irregularities at higher altitudes are highly anisotropic, i.e., the eddies become more flattened laterally. Along the vertical, the refractivity variation is mainly dominated by an exponential decay [71], but this is not the case along the horizontal direction. Besides, the repartition of the lines-of-sight in the sky can be scarce or uneven. For example, the GPS constellation, the most used one because of the high quality of its orbit modeling, offer quasi-repeating repeating tracks where only a few satellites (4 to 12) are visible from a particular location (**Figure 2**). This means that only a few lines-of-sight can be used at any time, and that there is, from a practitioner point of view, not enough data to constraint a better representation of the slant delays than the six-parameters Eq. (1).

Hopefully, Augmented Constellations and Low-Earth-Orbits constellations (LEO) will become soon a reality [72–74], thanks to the ever-decreasing size and costs of satellites, as well as the availability of miniaturized atomic clocks [75]. LEO constellations are particularly interesting for GNSS meteorology, as their satellites will cross the sky in a few minutes instead of hours, with a boost by one order of magnitude, or even two, of the available line-of-sight geometries. Our proposal to keep the separation of the refractivity into a "hydrostatic" and "wet" part, with the "hydrostatic" slant part evaluated separately from proven models like the Saastamoinen [41] model and subtracted from the total slant delay, then to represent the wet refractivity field based on a mean exponential decay of the wet refractivity as

$$\delta n_w(r) = N_w \exp\left(\frac{r - r_0}{H_w}\right)(1. + \varepsilon_w(x, y, z, t)) \tag{18}$$

where the ϵ_w terms represent the departure of the wet refractivity field from the exponential local decay law and x, y, z, t are local coordinates with respect to a frame linked with the local GNSS receiver and t is time. As the wet scale height can vary by a factor of four, it must be provided from external sources (for example from the ECMWF-ERA series of climate models, see [76]). An estimate of H_w can also be determined from the slant wet delays themselves, but only if a reliable estimate of the wet refractivity is available, as the integral over the geometrical path between the GNSS satellite and the receiver is proportional to $N_w H_w$ for a pure exponential decay of the wet refractivity. Empirical relations also exist between the ground value of the refractivity and scale height for example [77], but they are probably out-of-date. H_w is by itself a very important parameter, as [71] demonstrated that

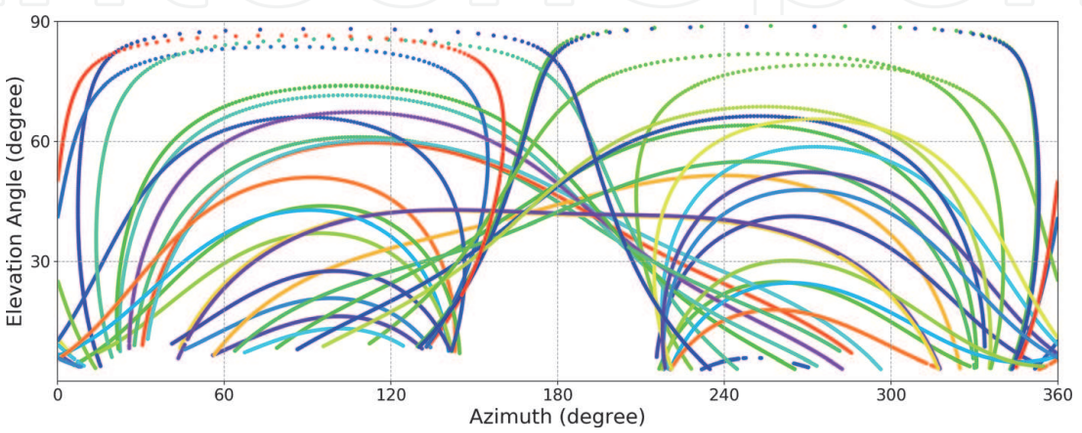

Figure 2.
The sky-tracks (in elevation and azimuth) of the GPS satellites (one color per satellite) visible from the THTI station (latitude: 17.5769° S, longitude: 149.6063° W), in the wet season on January 10th, 2018.

this scale height is related to the rate at which the PW decorrelates with horizontal separation.

On the contrary of Davis et al. [10], we fully represent the term $\varepsilon_w(x,y,z,t)$ as a 3D (or 4D if the time is present) series expansion

$$\varepsilon_n(x,y,z,t) = \sum_n \lambda_n \Phi_n(x,y,z,t) \tag{19}$$

where the $\Phi_n(x,y,z,t)$ are a set of suitably chosen orthogonal functions in the atmospheric lens comprised between the local horizon of the station and the local tropopause. The λ_n are the coefficients of the expansion. If the shape of the tropopause boundary is known [78], the Φ_n functions can be defined as empirical orthogonal functions (EOF) [79] or as a pre-defined set of orthogonal functions renormalized according to the Gram-Schmidt scheme [80].

A preliminary attempt with a small data set was made by [81] with the assumption of a constant altitude tropopause (see **Figure 3**), where the Φ_n orthogonal functions are a subset of Zernike functions [82]. The line-of-sight are assumed to be straight-lines to obtain tractable equations, as it is the case for tomography [83, 84] and the statistical analysis of the slant delays [85, 86]. This implies that low-elevation rays cannot be taken into account.

The integral relation to be solved with respect to ϵ_w is therefore

$$\delta L_w(e_0) = N_w \int_{\substack{geometrical \\ path}} \exp\left(\frac{r-r_0}{H_w}\right)(1. + \varepsilon_w(x,y,z,t))\, ds \tag{20}$$

This integral relationship is averaging the wet refractivity field along the lines-of-sight (fan-beam tomography [87, 88]), and the inversion in terms of λ_n coefficients must be regularized. By construction, the ε_w correction must be small, so we can use a truncated Singular Value decomposition (the EOF approach) or a Tikhonov approach [89] to enforce this smallness with respect to 1. The use of a priori refractivity values along the vertical for sites collocated with radiosoundings can also be envisaged [90] (in preparation). The Tikhonov approach, and its ability to model local variations of the refractivity field has been investigated in the framework of radar tomography [87, 91, 92].

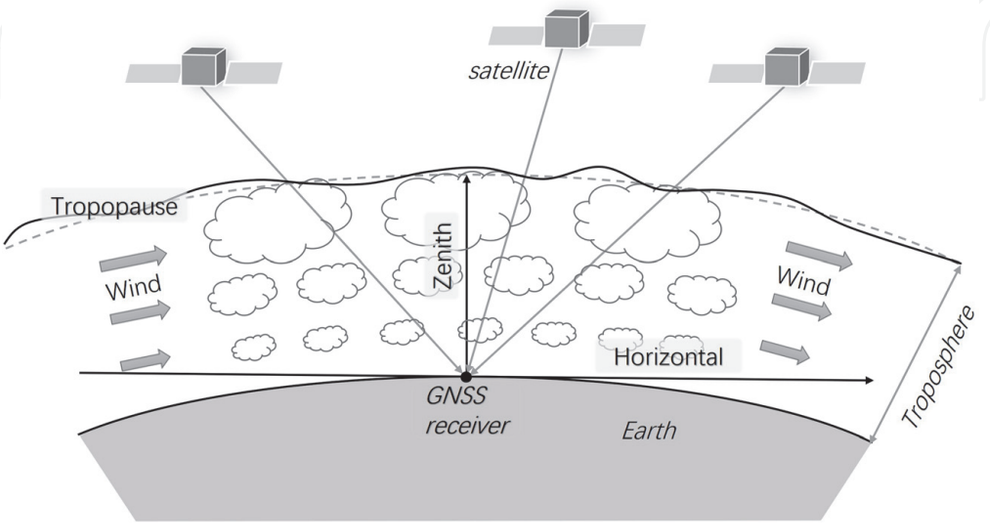

Figure 3.
The geometry of the inversion of the wet delays, with the representation of eddies in the troposphere, flattened with altitude and pushed by the wind [62, 63].

The only case where the hypothesis of a small ϵ_w can be violated occurs during inversion episodes, where atmospheric temperature increases when altitude increases. The warm inversion layer then acts as a cap and stops atmospheric mixing [93] causing a large deviation of the refractivity with respect to the exponential decay.

The end-product for the meteorology community of the inversion of Eq. (19) cannot only be the set of H_w and λ_n coefficients, that are too difficult to handle. We propose, in addition, to give the results in the form of records over a grid the resolution of which is in agreement with the maximum degree of the expansion in Eq. (19), with respect to a suitable ellipsoid (like WGS84), and with these fields:

Observation Time, Latitude, Longitude, Geometrical height, total refractivity, wet refractivity.

The refractivity fields can then be converted, if needed, to water vapor levels according to Eq. (6) with suitable temperature profiles over the troposphere and/or feed high resolution NWM taking natively into account turbulent/convective processes [94]. Xia et al. [95] tried to derive the refractivity field from slant delays by substituting Eq. (6) into Eq. (9), but the underlying hypothesis is an atmosphere at rest, in a similar fashion of the neutral delay model of Saastamoinen [41, 96].

Is the approach developed in this article directly implementable in GNSS software, as a replacement of the usual approach of Eq. (1)? The response is a careful yes [69]. Strictly speaking, a mapping function defines, from the point of view of differential geometry, a time-evolving coordinate chart that is a non-orthogonal system of coordinates made of the refracted elevation at ground level, the length along the bended ray, and the azimuth. We think that such an implementation in GNSS software implies at least the use of a constant (i.e., not evolving with time) system of coordinates (i.e., a constant mapping function), that therefore must be computed with respect to some standard model of the atmosphere, carefully designed and normalized [97]. For this purpose, it should be noted that the variation of the propagation delay caused by the bending is of second order with respect to the integration of the refractivity along the path [98].

Finally, the modeling of the wet refractivity field through an expansion series in time and space (Eq. (19)) can be also used to model tropospheric delays, in a correlated way, between uplink and downlink signals to planetary space crafts, where the uplink and downlink separation in time can reach tens of minutes or even hours [99].

5. Conclusion

We discussed in this brief paper the pros and cons of the standard approach mapping functions + gradients to model the neutral delays of the atmosphere, and more specifically the wet delays caused by the presence of water vapor in the troposphere. If this standard approach is almost perfect for people doing positioning, deformation and VLBI studies, as they see the neutral delays as “noise”, it is not so well adapted to people looking at these delays as signals to study atmospheric processes. In particular, the standard definition of gradients is too crude, and does not permit to have access to the horizontal turbulence/convection scales, that are key parameters to model these processes in high resolution NWM models. We therefore propose an alternative way to model the wet tropospheric delays, through a representation of the wet refractivity field as a perturbation over an exponential decay with altitude with a locally adjusted scale height and a time/space series expansion over a suitable basis of orthogonal functions. Our approach is computationally expensive, and maybe not suited for real-time applications, but its

end-product are records of the total and wet refractivity values with high-resolution in time (minute-scale) and distance (sub km-scale), in accordance with the needs of future numerical weather models [38], the emerging field of the modeling of atmospheric rivers [100, 101] and besides does not require the additional step of water vapor tomography, with lower cost, better mobility and simpler operation [102].

Acknowledgements

This research was funded by a DAR grant from the French Space Agency (CNES) to the Geodesy Observatory of Tahiti. Feng Peng did this research in the framework of his Ph.D., with a 14-months stay at the Observatory of Tahiti funded through the Cai Yuanpei program.

Conflict of interest

The authors declare no conflict of interest.

Author details

Jean-Pierre Barriot[1*] and Peng Feng[2]

1 University of French Polynesia, French Polynesia

2 LIESMARS State Key Laboratory, Wuhan University, China

*Address all correspondence to: jean-pierre.barriot@upf.pf

References

[1] Flores A, Ruffini G, Rius A. 4D tropospheric tomography using GPS slant wet delays. Ann Geophys. 2000;18 (2):223–34.

[2] Webb FH, Zumberge JF. An introduction to GIPSY/OASIS-II precision software for the analysis of data from the Global Positioning System. Pasadena, California; 1995.

[3] Dach, R., S. Lutz, P. Walser PF (Eds). Bernese GNSS Software Version 5.2. Vol. 2, Astronomical Institute, University of Bern. Bern, Switzerland: University of Bern, Bern Open Publishing; 2015. 826 p.

[4] O'Driscoll Cillian. Carrier phase and its measurement for GNSS. GNSS Insider [Internet]. 2010 [cited 2021 Jan 16]; Available from: www.insidegnss.com

[5] Nikolaidou T, Balidakis K, Nievinski F, Santos M, Schuh H. Impact of different NWM-derived mapping functions on VLBI and GPS analysis. Earth, Planets Sp. 2018 Dec 1;70(1):1–16.

[6] Marini JW. Correction of Satellite Tracking Data for an Arbitrary Tropospheric Profile. Radio Sci. 1972 Feb 1;7(2):223–31.

[7] Davis JL, Herring TA, Shapiro II, Rogers AEE, Elgered G. Geodesy by radio interferometry: Effects of atmospheric modeling errors on estimates of baseline length. Radio Sci. 1985 Nov 1;20(6):1593–607.

[8] Herring TA. Modeling Atmospheric Delays in the Analysis of Space Deodetic Data. In: Symposium on Refraction of Transatmospheric Signals in Geodesy, 19–22 May 1992. Delft, Netherlands: Netherlands Geodetic Commission Publications on Geodesy; 1992. p. 157–64.

[9] Nilsson T, Böhm J, Wijaya DD, Tresch A, Nafisi V, Schuh H. Path Delays in the Neutral Atmosphere. In: Atmospheric Effects in Space Geodesy. Springer, Berlin, Heidelberg; 2013. p. 73–136.

[10] Davis JL, Elgered G, Niell AE, Kuehn CE. Ground-based measurement of gradients in the "wet" radio refractivity of air. Radio Sci. 1993;28(6):1003–18.

[11] MacMillan DS. Atmospheric gradients from very long baseline interferometry observations. Geophys Res Lett. 1995;22(9):1041–4.

[12] Chen G, Herring TA. Effects of atmospheric azimuthal asymmetry on the analysis of space geodetic data. J Geophys Res Solid Earth. 1997;102(B9): 20489–502.

[13] Boehm J, Werl B, Schuh H. Troposphere mapping functions for GPS and very long baseline interferometry from European Centre for Medium-Range Weather Forecasts operational analysis data. J Geophys Res Solid Earth. 2006;111(2):1–9.

[14] Landskron D, Böhm J. VMF3/GPT3: refined discrete and empirical troposphere mapping functions. J Geod. 2018;92(4):349–60.

[15] Rüeger JM. Refractive Index Formulae for Radio Waves. In: FIG Technical Program. Washington, D.C. USA: FIG XXII International Congress; 2002. p. 1–13.

[16] Stevens B, Brogniez H, Kiemle C, Lacour J-L, Crevoisier C, Kiliani J. Structure and Dynamical Influence of Water Vapor in the Lower Tropical Troposphere. In Springer, Cham; 2017. p. 199–225.

[17] McGuffie K, Henderson-Sellers A. A Climate Modelling Primer. Chichester, UK: John Wiley & Sons, Ltd; 2005. 1–280 p.

[18] Stocker T. Model Hierarchy and Simplified Climate Models. In: Introduction to Climate Modelling. Springer-Verlag Berlin Heidelberg; 2011. p. 25–51.

[19] Dessler AE, Sherwood SC. A matter of humidity. Science (80-). 2009;323 (5917):1020–1.

[20] Schmidt GA, Ruedy RA, Miller RL, Lacis AA. Attribution of the present-day total greenhouse effect. J Geophys Res Atmos. 2010 Oct 27;115(20).

[21] Hansen J, Sato M, Ruedy R, Kharecha P, Lacis A, Miller R, et al. Dangerous human-made interference with climate: a GISS modelE study. Atmos Chem Phys. 2007 May 7;7(9): 2287–312.

[22] Elliott WP, Gaffen DJ. Chapman Conference Probes Water Vapor in the Climate System. In: Eos, Transactions American Geophysical Union. John Wiley & Sons, Ltd; 1995. p. 67–67.

[23] King MD, Kaufman YJ, Menzel WP, Tanré D. Remote Sensing of Cloud, Aerosol, and Water Vapor Properties from the Moderate Resolution Imaging Spectrometer (MODIS). IEEE Trans Geosci Remote Sens. 1992;30(1):2–27.

[24] Whiteman DN, Melfi SH, Ferrare RA. Raman lidar system for the measurement of water vapor and aerosols in the Earth's atmosphere. Appl Opt. 1992 Jun 1;31(16):3068.

[25] Halthore RN, Eck TF, Holben BN, Markham BL. Sun photometric measurements of atmospheric water vapor column abundance in the 940-nm band. J Geophys Res Atmos. 1997 Feb 27;102(4):4343–52.

[26] Cimini D, Campos E, Ware R, Albers S, Giuliani G, Oreamuno J, et al. Thermodynamic atmospheric profiling during the 2010 winter olympics using ground-based microwave radiometry. IEEE Trans Geosci Remote Sens. 2011 Dec;49(12 PART 2):4959–69.

[27] Durre I, Vose RS, Wuertz DB. Overview of the integrated global radiosonde archive. J Clim. 2006 Jan 15; 19(1):53–68.

[28] Van Baelen J, Reverdy M, Tridon F, Labbouz L, Dick G, Bender M, et al. On the relationship between water vapour field evolution and the life cycle of precipitation systems. Q J R Meteorol Soc. 2011 Jan 1;137(S1):204–23.

[29] Koulali A, Ouazar D, Bock O, Fadil A. Study of seasonal-scale atmospheric water cycle with ground-based GPS receivers, radiosondes and NWP models over Morocco. Atmos Res. 2012 Feb 1;104–105:273–91.

[30] Brenot H, Ducrocq V, Walpersdorf A, Champollion C, Caumont O. GPS zenith delay sensitivity evaluated from high-resolution numerical weather prediction simulations of the 8–9 September 2002 flash flood over southeastern France. J Geophys Res. 2006 Aug 16;111(D15):D15105.

[31] Uppala SM, Kållberg PW, Simmons AJ, Andrae U, da Costa Bechtold V, Fiorino M, et al. The ERA-40 re-analysis. Q J R Meteorol Soc. 2005 Oct 1;131(612):2961–3012.

[32] Marini JW, Murray CW. Correction of laser range tracking data for atmospheric refraction at elevations above 10 degrees. Goddard Space Flight Center, Greenbelt, Maryland: NASA Technical Report; 1973.

[33] Thayer GD. A Rapid and Accurate Ray Tracing Algorithm for a Horizontally Stratified Atmosphere. Radio Sci. 1967;2(2):249–52.

[34] Thompson DA, Pepin TJ, Simon FW. Ray Tracing in Refracting Spherically Symmetric Atmosphere. J Opt Soc Am. 1982;72(11):1498–501.

[35] Smith EK, Weintraub S. The Constants in the Equation for Atmospheric Refractive Index at Radio Frequencies. Proc IRE. 1953;41(8):1035–7.

[36] Boudouris G. On the index of refraction of air, the absorption and dispersion of centimeterwaves by gases. J Res Natl Bur Stand Sect D Radio Propag. 1963;67D(6):631.

[37] Bevis M. GPS meteorology: mapping zenith wet delays onto precipitable water. Vol. 33, Journal of Applied Meteorology. 1994. p. 379–86.

[38] Bauer P, Thorpe A, Brunet G. The quiet revolution of numerical weather prediction. Vol. 525, Nature. Nature Publishing Group; 2015. p. 47–55.

[39] Stevens B. Atmospheric moist convection. Vol. 33, Annual Review of Earth and Planetary Sciences. Annual Reviews; 2005. p. 605–43.

[40] Steppeler J, Hess R, Schättler U, Bonaventura L. Review of numerical methods for nonhydrostatic weather prediction models. Meteorol Atmos Phys. 2003 Jan;82(1–4):287–301.

[41] Saastamoinen J. Atmospheric Correction for the Troposphere and Stratosphere in Radio Ranging Satellites. In: Geophysical Monograph Series. 1972. p. 247–51.

[42] Butler B. Precipitable water at KP 1993–1998, MMA MEMO 238 [Internet]. 1998 [cited 2021 Jan 14]. Available from: https://library.nrao.edu/public/memos/alma/main/memo238.pdf

[43] Zhang B, Yao Y, Xu C. Global empirical model for estimating water vapor scale height. Cehui Xuebao/Acta Geod Cartogr Sin. 2015 Oct 1;44(10):1085.

[44] Reid GC, Gage KS. On the annual variation in height of the tropical tropopause. J Atmos Sci. 1981 Sep 1;38 (9):1928–38.

[45] Tomikawa Y, Nishimura Y, Yamanouchi T. Characteristics of Tropopause and Tropopause Inversion Layer in the Polar Region. SOLA. 2009;5 (1):141–4.

[46] Minzner RA, Reber CA, Jacchia LG, Huang FT, Cole AE, Kantor AJ, et al. Defining Constants, Equations, and Abbreviated Tables of the 1975 U.S. Standard Atmosphere. NASA Technical Report R-459; 1976.

[47] Fleming EL, Chandra S, Barnett JJ, Corney M. Zonal mean temperature, pressure, zonal wind and geopotential height as functions of latitude. Adv Sp Res. 1990;

[48] ITU-R. The radio refractive index : its formula and refractivity data. Vol. P.453–11, Radiocommunication Sector of IUT. 2015.

[49] Bar-Sever YE, Kroger PM, Borjesson JA. Estimating horizontal gradients of tropospheric path delay with a single GPS receiver. J Geophys Res Solid Earth. 1998 Mar 10;103(B3): 5019–35.

[50] MacMillan DS, Ma C. Atmospheric gradients and the VLBI terrestrial and celestial reference frames. Geophys Res Lett. 1997;24(4):453–6.

[51] Graffigna V, Hernández-Pajares M, Gende M, Azpilicueta F, Antico P. Interpretation of the Tropospheric Gradients Estimated With GPS During Hurricane Harvey. Earth Sp Sci. 2019;6 (8):1348–65.

[52] Bevis M, Businger S, Herring TA, Rocken C, Anthes RA, Ware RH. GPS meteorology: remote sensing of atmospheric water vapor using the global positioning system. J Geophys Res. 1992;97(D14):15787.

[53] Hirahara K. Local GPS tropospheric tomography. Earth, Planets Sp. 2000;52 (11):935–9.

[54] de Haan S, van der Marel H. Observing three dimensional water vapour using a surface network of GPS receivers. Atmos Chem Phys Discuss. 2008 Sep 11;8(5):17193–235.

[55] Morel L, Pottiaux E, Durand F, Fund F, Boniface K, De Oliveira PS, et al. Validity and behaviour of tropospheric gradients estimated by GPS in Corsica. Adv Sp Res. 2015;55(1): 135–49.

[56] Nahmani S, Bock O, Guichard F. Sensitivity of GPS tropospheric estimates to mesoscale convective systems in West Africa. Atmos Chem Phys. 2019;19(14):9541–61.

[57] Guerova G, Jones J, Douša J, Dick G, De Haan S, Pottiaux E, et al. Review of the state of the art and future prospects of the ground-based GNSS meteorology in Europe. Atmos Meas Tech. 2016;9 (11):5385–406.

[58] Douša J, Dick G, Kačmařík M, Bro Řková R, Zus F, Brenot H, et al. Benchmark campaign and case study episode in central Europe for development and assessment of advanced GNSS tropospheric models and products. Atmos Meas Tech. 2016 Jul 14;9(7):2989–3008.

[59] Järvinen H, Eresmaa R, Vedel H, Salonen K, Niemelä S, de Vries J. A variational data assimilation system for ground-based GPS slant delays. Q J R Meteorol Soc. 2007 Apr 1;133(625):969–80.

[60] Hdidou FZ, Mordane S, Moll P, Mahfouf J-F, Erraji H, Dahmane Z. Impact of the variational assimilation of ground-based GNSS zenith total delay into AROME-Morocco model. Tellus A Dyn Meteorol Oceanogr. 2020 Jan 1;72(1):1–13.

[61] Haynes PH. Transport and Mixing in the Atmosphere. In: Mechanics of the 21st Century. Dordrecht: Springer; 2005. p. 139–52.

[62] Holton JR, Hakim GJ. An introduction to dynamic meteorology: Fifth edition. Vol. 9780123848. Academic Press; 2012. 1–552 p.

[63] Foken T. 50 years of the Monin-Obukhov similarity theory. Vol. 119, Boundary-Layer Meteorology. Springer; 2006. p. 431–47.

[64] Xue H, Feingold G. Large-eddy simulations of trade wind cumuli: Investigation of aerosol indirect effects. J Atmos Sci. 2006;63(6):1605–22.

[65] Neggers RAJ, Jonker HJJ, Siebesma AP. Size statistics of cumulus cloud populations in large-eddy simulations. J Atmos Sci. 2003;60(8): 1060–74.

[66] Schöck M, Spillar EJ. Method for a quantitative investigation of the frozen flow hypothesis. J Opt Soc Am A. 2000; 17(9):1650.

[67] Schulz-DuBois EO, Rehberg I. Structure function in lieu of correlation function. Appl Phys. 1981 Apr;24(4): 323–9.

[68] Bobak JP, Ruf CS. A new model for the structure function of integrated water vapor in turbulence. Radio Sci. 1999 Nov 1;34(6):1461–73.

[69] Zhang F, Barriot J, Xu G, Hopuare M. Modeling the Slant Wet Delays From One GPS Receiver as a Series Expansion With Respect to Time and Space: Theory and an Example of Application for the Tahiti Island. IEEE Trans Geosci Remote Sens. 2020;1–13.

[70] Halsig S, Artz T, Iddink A, Nothnagel A. Using an atmospheric turbulence model for the stochastic model of geodetic VLBI data analysis 6. Geodesy. Earth, Planets Sp. 2016 Dec 1; 68(1):1–14.

[71] Ruf CS, Beus SE. Retrieval of tropospheric water vapor scale height

from horizontal turbulence structure. IEEE Trans Geosci Remote Sens. 1997;35 (2):203–11.

[72] Li X, Li X, Ma F, Yuan Y, Zhang K, Zhou F, et al. Improved PPP Ambiguity Resolution with the Assistance of Multiple LEO Constellations and Signals. Remote Sens. 2019 Feb 17;11(4):408.

[73] Li X, Zus F, Lu C, Ning T, Dick G, Ge M, et al. Retrieving high-resolution tropospheric gradients from multiconstellation GNSS observations. Geophys Res Lett. 2015;42(10):4173–81.

[74] Wei H, Li J, Zhang S, Xu X. Cycle Slip Detection and Repair for Dual-Frequency LEO Satellite GPS Carrier Phase Observations with Orbit Dynamic Model Information. Remote Sens. 2019 May 29;11(11):1273.

[75] Ely TA, Burt EA, Prestage JD, Seubert JM, Tjoelker RL. Using the Deep Space Atomic Clock for Navigation and Science. IEEE Trans Ultrason Ferroelectr Freq Control. 2018 Jun 1;65 (6):950–61.

[76] Kennett EJ, Toumi R. Temperature dependence of atmospheric moisture lifetime. Geophys Res Lett. 2005 Oct 16; 32(19):1–4.

[77] Bean BR, Thayer GD. Models of the Atmospheric Radio Refractive Index. Proc IRE. 1959;47(5):740–55.

[78] Hoerling MP, Schaack TK, Lenzen AJ. Global objective tropopause analysis. Mon Weather Rev. 1991 Aug 1; 119(8):1816–31.

[79] Zhang Z, Moore JC. Mathematical and Physical Fundamentals of Climate Change. Elsevier; 2015. 1–494 p.

[80] Arfken G, Romain JE. 9.3 Gram-Schmidt Orthogonalization. In: Mathematical Methods for Physicists 3rd Edition. Academic Press; 1985. p. 516–20.

[81] Barriot J-P, Serafini J, Sichoix L. Estimating the 3D Time Variable Water Vapor Contents of the Troposphere from a Single GNSS Receiver. In: International Conference on Earth Observations & Societal Impact. Tainan, Taiwan: Taiwan group on Earth Observations; 2013. arXiv: 2102.01858.

[82] Mathar RJ. Zernike basis to Cartesian transformations. Serbian Astron J. 2009;179(179):107–20.

[83] Flores A, Gradinarsky LP, Elósegui P, Elgered G, Davis JL, Rius A. Sensing atmospheric structure: Tropospheric tomographic results of the small-scale GPS campaign at the Onsala Space Observatory. Earth, Planets Sp. 2000;52(11):941–5.

[84] Bender M, Stosius R, Zus F, Dick G, Wickert J, Raabe A. GNSS water vapour tomography - Expected improvements by combining GPS, GLONASS and Galileo observations. Adv Sp Res. 2011; 47(5):886–97.

[85] Wheelon AD. Electromagnetic scintillation. Volume 1, Geometrical optics. Cambridge University Press; 2001. 455 p.

[86] Schön S, Brunner FK. Atmospheric turbulence theory applied to GPS carrier-phase data. J Geod. 2008 Jan;82(1):47–57.

[87] Barriot JP, Kofman W, Herique A, Leblanc S, Portal A. A two dimensional simulation of the CONSERT Experiment (radio tomography of comet Wirtanen). Adv Sp Res. 1999 Jan 1;24(9):1127–38.

[88] Peng H, Stark H. Direct Fourier Reconstruction in Fan-Beam Tomography. IEEE Trans Med Imaging. 1987 Sep;6(3):209–19.

[89] Menke W. Geophysical data analysis: Discrete inverse theory. Academic Press; 2012. 1–352 p.

[90] Feng P, Zhang F, Li F, Yan J, Barriot J-P. Line of Sight Wet

Refractivity from a single GNSS Receiver (in preparation). 2021.

[91] Benna M, Barriot JP, Kofman W. A priori information required for a two or three dimensional reconstruction of the internal structure of a comet nucleus (CONSERT experiment). Adv Sp Res. 2002 Mar 1;29(5):715–24.

[92] Benna M, Piot A, Barriot JP, Kofman W. Data set generation and inversion simulation of radio waves propagating through a two-dimensional comet nucleus (CONSERT experiment). Radio Sci. 2002;37(6):3–1–3–16.

[93] Wallace JM, Hobbs P V. Atmospheric Science: An Introductory Survey: Second Edition. Atmospheric Science: An Introductory Survey: Second Edition. Elsevier Inc.; 2006. 1–488 p.

[94] Hanna N, Trzcina E, Möller G, Rohm W, Weber R. Assimilation of GNSS tomography products into the Weather Research and Forecasting model using radio occultation data assimilation operator. Atmos Meas Tech. 2019 Sep 10;12(9):4829–48.

[95] Xia P, Ye S, Guo M, Jiang W, Xu C. Retrieval of Tropospheric Refractivity Profiles Using Slant Tropospheric Delays Derived From a Single Ground-Based Global Navigation Satellite System Station. Earth Sp Sci. 2019 Jul 1; 6(7):1081–97.

[96] Saastamoinen J. Contributions to the theory of atmospheric refraction - Part II. Refraction corrections in satellite geodesy. Bull Géodésique. 1973;47(1): 428.

[97] Minzner RA. The 1976 Standard Atmosphere and its relationship to earlier standards. Rev Geophys. 1977;15 (3):375–84.

[98] Zernov N, Lundborg B. The statistical theory of wave propagation and HF propogation in the ionosphere with local inhomogeneities. Swedish Institute of Space Physics; 1993.

[99] Thornton CL, Border JS. Radiometric Tracking Techniques for Deep Space Navigation. Border: Wiley; 2003.

[100] Payne AE, Demory M-E, Leung LR, Ramos AM, Shields CA, Rutz JJ, et al. Responses and impacts of atmospheric rivers to climate change. Nat Rev Earth Environ. 2020 Mar 9;1 (3):143–57.

[101] Lavers DA, Ralph FM, Richardson DS, Pappenberger F. Improved forecasts of atmospheric rivers through systematic reconnaissance, better modelling, and insights on conversion of rain to flooding. Commun Earth Environ. 2020 Dec 28;1(1):1–7.

[102] Lin L, Zhao Z, Zhu Q, Zhang Y. Profiling tropospheric refractivity in real time, based on a relevance vector machine and single ground-based GPS receiver. Int J Remote Sens. 2012;33(13): 4044–58.